SYNERGISTIC EFFECTS OF HEATED WALNUT SHELL POWDER AND REDUCED GRAPHENE OXIDE IN PARAFFIN WAX COMPOSITES FOR MARINE THERMAL APPLICATIONS

Reference NO. IJME 1359, DOI: 10.5750/ijme.v1i1.1359

Aman Sharma*, Department of Mechanical Engineering, GLA University, Mathura, India, **Pradeep Kumar Singh,** Department of Mechanical Engineering, GLA University, Mathura, India and **Kamal Sharma**, Department of Mechanical Engineering, GLA University, Mathura, India

* Corresponding author. Aman Sharma (Email): aman.sharma@gla.ac.in

KEY DATES: Submission date: 02.09.2023 / Final acceptance date: 20.02.2024 / Published date: 12.07.2024

SUMMARY

The study focuses on creating and analyzing paraffin wax composites enriched with heated walnut shell powder and reduced graphene oxide nanoparticles. Experimental procedures include careful blending of materials to form homogeneous mixtures, followed by analysis using techniques such as thermal gravimetric analysis (TGA), scanning electron microscopy (SEM), X-ray photoelectron spectroscopy (XPS), Fourier transform infrared spectroscopy (FTIR), and differential scanning calorimetry (DSC). The composites show improved thermal properties compared to pure paraffin wax, with increased melting temperatures, heat of fusion, and thermal conductivity. The study also examines density and thermal diffusivity, providing insights into thermal behavior. Additionally, it ensures the corrosion resistance of nano-enhanced bio-based phase change materials (PCMs) for marine engineering through thorough material selection, corrosion testing, and long-term exposure studies simulating seawater conditions. The study evaluates environmental impacts, toxicity, and compliance with standards and proposes mitigation strategies like protective coatings and encapsulation techniques. Overall, the research contributes to developing environmentally sustainable PCM materials for marine applications and offers insights into their thermal behavior for thermal energy storage and management.

KEYWORDS

Walnut shell, Paraffin wax, Characterization, XRD, SEM, FTIR, Nano enhanced bio-based PCM, Marine application

1. INTRODUCTION

The world's energy consumption is rising rapidly, making it necessary to use renewable energy sources, improve energy efficiency, and reduce greenhouse gas emissions. Thermal energy storage (TES) is one of the easiest and cheapest techniques to improve energy management (Cárdenas-Ramírez et al., 2020; Li et al., 2020). To eliminate PCM leakage, form-stable composite PCMs were suggested. This packaging uses PCM-supporting material. Clay (natural clay, perlite, and bentonite), polymers (polyurethane, high/low-density polyethylene), and industrial waste have been investigated to fix the shape. PCMs were evaluated with extra resources. PCMs are protected by such liquid, weatherproof materials. A supporting material reduces composite PCM heat storage capacity (Alkhazaleh, 2020; Aslfattahi et al., 2020; Chen et al., 2014; da Cunha and de Aguiar, 2020; Huang et al., 2017; Liu et al., 2019; Navarro et al., 2017; Tang et al., 2016). Advanced thermal-enhanced composite PCMs coat porous, heat-conductive matrices with PCM. A bio-carbon PCM hosting matrix's benefits. Low density, high sorption capacity, affordability, environmental friendliness, and excellent thermal stability and conductivity (Atinafu et al., 2020a, 2020b; Jeon et al., 2019; Ranjbar et al., 2020).

In marine engineering, phase change materials (PCMs) are promising. They can be combined into maritime anti-corrosion coatings to create useful, high-performing, eco-friendly, and energy-efficient goods (Rossi et al., 2022; Zhong et al., 2022). Study results have examined the biofouling and durability of carbon nanotubes (CNTs) in maritime environments (Yadav et al., 2023). Cyanoacrylate-coated CNTs may be stronger and biofouling-resistant. Eco-friendly marine coatings like SiNC decrease biocides' toxicity to non-target marine life. Finally, nanobiotechnology and bioremediation clean the ocean sustainably with marine microorganisms and bio-generated nanomaterials (Wu and Lv, 2022; Zhang and Zhao, 2020). The maritime sector is focusing on energy. Since pressurization is inefficient, compressed air is a useful energy source. System performance depends on operating pressure and leakage rate (Dere and Deniz, 2019). In order to assess risk and present any options for the LNG tank cooling process, a thorough understanding of heat transport characteristics is necessary (Deng et al., 2020).

Using carbon derived from biomass, aerogels were able to transport palmitic acid and 1-hexadecanamine (Wang et al., 2020). Outstanding thermal properties were achieved by combining carbonized wood with 1-tetradeconal as a PCM (Yang et al., 2018). A composite material was produced by impregnating carbonized abandoned rice with a palmitic-lauric acid eutectic combination (Zhang et al., 2017). This composite material had excellent LHTES. Impregnating n-octadecane with activated carbon from palm kernel shells produced a shape-stabilized composite PCM (Feng et al., 2011). Different molecular weights of polyethylene glycol (PEG) were shown to be sustained when activated carbon generated from coconuts was used (Nicholas et al., 2018). Chemical activation on PCM absorption, LHTES, thermal conductivity, and thermal energy storage/release was compared using ZnCl2 solution and WS carbonization. Activator ZnCl2 was employed. A high temperature (400-600◦C) activation of $ZnCl^2$ results in a microporous carbon structure with enhanced surface area and volume. Hole formation from bio-carbon and aromatic graphitic structure breakdown can enhance carbon content (Hock and Zaini, 2018; Lee et al., 2019; Shan et al., 2020).

From residual vegetable and animal fats, organic fatty acid ester compounds are bio-based PCMs. Innovative organic PCMs are less flammable than paraffins. Bio-based mass-produced PCMs cost higher than paraffins. Construction materials retain thermal energy well. TES's growing role in the energy transition and future energy storage materials make PCMs non-depletable resources important for a sustainable energy future. Biodegradable and compostable PCMs could enhance TES sustainability (Liu et al., 2020; Lu et al., 2019). Bio-based PCMs are new, yet plastic making has employed them for decades. Produced and sustainable like fossil-based plastics, bio-based polymers are not biodegradable or compostable. Animal/fish, tropical, or vegetable fats are in bio-based PCM? While each bio-based PCM must be tested, biodegradability is expected. Most biobased PCMs are safe at -80 to 275°C (Baylis and Cruickshank, 2023; Jeong et al., 2013).

2. EXPERIMENTATION

To prepare samples of paraffin wax composites enriched with heated walnut shell powder, each incorporated with graphene nanoparticles for subsequent measurements of thermal conductivity, melting temperature, and enthalpy at varying heating rates and weight percentages, a precise protocol is followed as shown in Figure 1 and Table 1. Paraffin wax and heated powder (walnut shell) are precisely weighed, with the possibility to increase the heated powder weight from 5% to 20%. Homogeneously combine the hot powder with paraffin wax. Next, graphene nanoparticles are combined with paraffin wax and heated powder to achieve weight percentages of 0.01% to 0.1%. By gently mixing the liquid, nanoparticles are equally disseminated. Place the composite in a copper or aluminium sample container.

Figure 1. (a) Heat treatment process for walnut shell (b) Magnetic stirring process and material

Table 1. Different sample composition of wall nut shell

Sample	**Ferrocene**	**WS%**	**Yield**
1	0.1 (17%)	0.5	0.1624g
2	0.2 (34%)	0.4	0.1275 g
3	0.3 (51%)	0.3	0.0785 g
4	0.4 (68%)	0.2	0.0480g
5	Wall nutshell		
Sample 6	Heat treated in nitrogen gas environment wall nutshell 800 °C for 3 hours		
Sample 7	HNWS Heat Treated in Nitrogen Environment Walnut Shell With 5 Mol HNO_3 acid leaching		
Weight		5gm before	3.1501g after

Scan calorimeters hold this sample holder. DSC scans occur at specific heating rates. At each heating rate and weight percentage, weighting to DSC scanning is repeated. A brown, water-insoluble walnut processing by-product, walnut shell powder is heated. High heat capacity and thermal conductivity suggest renewable and biodegradability. As a filler, it improves paraffin wax composite thermal characteristics. Distribution graphene nanoparticles in the composite with a sonicitor. DSC scans in nitrogen reduce paraffin wax oxidation. DSC scans can calculate paraffin wax composites containing heated walnut shell powder and graphene nanoparticles' thermal conductivity, melting temperature, and enthalpy. Characterizing them helps understand their thermal properties and uses.

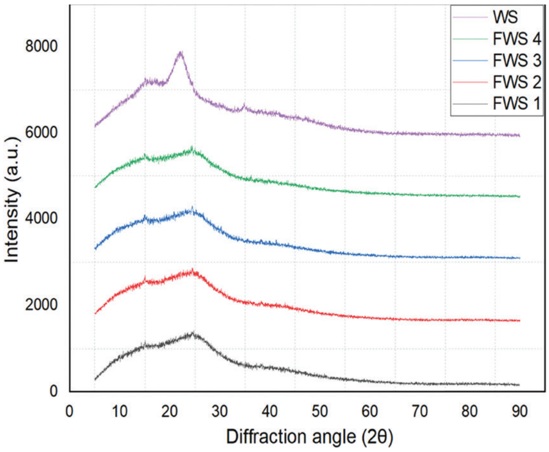

Figure 2. XRD patterns of ferrocene-containing samples (FWS) with varying ferrocene and water-soluble (WS) content

3. CHARACTERIZATION

3.1 X-RAY DIFFRACTION ANALYSIS

As seen in Figure 2, each sample's crystalline structures are identified by unique XRD peaks. To identify crystalline phases, diffraction angles (2θ) are essential due to the unique peak positions of each substance. The most noticeable peaks in the WS sample indicate a high amount of material in the X-ray diffracting phase or a preferred crystallite orientation. Sharper peaks suggest well-formed, big crystallites, while broader peaks may indicate lower crystallite sizes or higher crystal lattice macro strain. Pairing these qualities with sample details reveals nuance: FWS 1 yields 0.1624g and has intense peaks, indicating intermediate to high crystallinity with 17% Ferrocene and 0.5 WS%. In Sample 2 (FWS 2), peak intensity drops when Ferrocene is increased to 34% and WS% is dropped to 0.4, indicating structure modification and 0.1275 g yield. The much lower yield of 0.0785 g indicates that Ferrocene or its intrinsic non-crystalline character disrupts the crystalline phase, causing peak intensity to diminish further as Ferrocene concentration rises to 51% in Sample 3 (FWS 3) and WS% lowers to 0.3. The lowest yield of 0.0480g and maximum Ferrocene concentration of 68% and lowest WS% of 0.2 imply insignificant crystallinity or a considerable impact on the crystal structure, and the least sharp peaks indicate inhibitory activity. Ferrocene and WS% are shown to reduce XRD peak intensity and yield. Ferrocene concentrations may hinder crystallization or change the process to limit Figure 3 XRD crystalline phase growth. WS% may facilitate a reaction or crystalline structure.

3.2 FT-IR SPECTROSCOPY OF WALNUT SHELL

FT-IR spectroscopy, which can identify functional groups and frequencies between 500 and 4000 cm^{-1}, shows chemical bonding on walnut shells (WNS) before and after acid treatment. The raw WNS spectrum (Figure 3) showed numerous important peaks: 3322 cm^{-1}: A broad band of hydroxyl (OH) groups, possibly implicated in hydrogen bonding and adsorption. 2720-2509 cm^{-1}: This region had two peaks: one for aliphatic C-H stretching in organic compounds and one for ester group C=C double bonds. 1616-1589 cm^{-1}: C=O stretching vibrations showed ester, ether, and phenol groups in WNS. 1025-1078 cm^{-1}: Another C-O stretching area verifying ester, ether, and

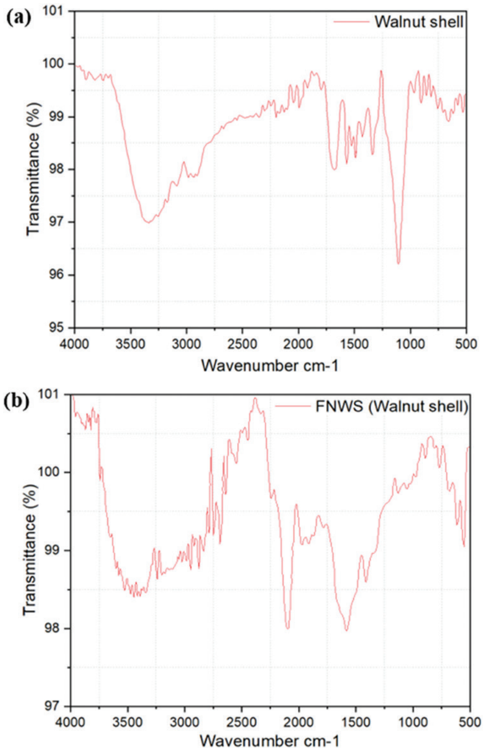

Figure 3. The FT-IR spectra of the walnut shell both before and after the acid activation process (a and b)

phenol functions. 867-590 cm^{-1}: C-H out-of-plane bending vibrations indicated benzene derivatives in medium peaks in this range. WNS raw and acid-treated spectra offered crucial information. Dye molecules may adsorb onto the WNS surface via functional groups like OH, C=C, and C-O.

FT-IR spectra changed significantly after acid treatment. Some peaks vanished, shrunk, or arose. Treatment with acid activation and higher temperatures likely disrupted WNS intermolecular interactions. The midrange peaks of 867-590 cm^{-1} survived following acid treatment, suggesting benzene derivatives in WNS structure despite surface modifications. Finally, a comprehensive FT-IR research demonstrated acid treatment greatly altered WNS surface chemistry. Disrupting intermolecular interactions and adding surface functionalities may have boosted dye adsorption. Acid-treated WNS may get rid of dye.

3.3 SCANNING ELECTRON MICROSCOPY

In Figure 4, the biochar's surface morphology, as determined by SEM analysis, is displayed. The biochar samples display various structural features: (a) porous cracks, (b) grains, (c) planner sheet-like structures, and (d) a rocky-like structure scattered throughout. Some of these structures are diverse and have rough surfaces. Biochar devolatilizes and alters morphologically due to high-rate heating releasing volatile components. This technique gives biochar samples a high-pore surface structure. SEM also evaluated the surface morphology and porous structure of Ferrocene-treated walnut shell (WNS) and bio-char (FNWS). Figure 4 shows that the rough, irregular surface has many macros and micropores of various sizes and shapes, creating multiple adsorption holes and gaps. A rough biochar surface may improve its surface area for adsorption of pollutants.

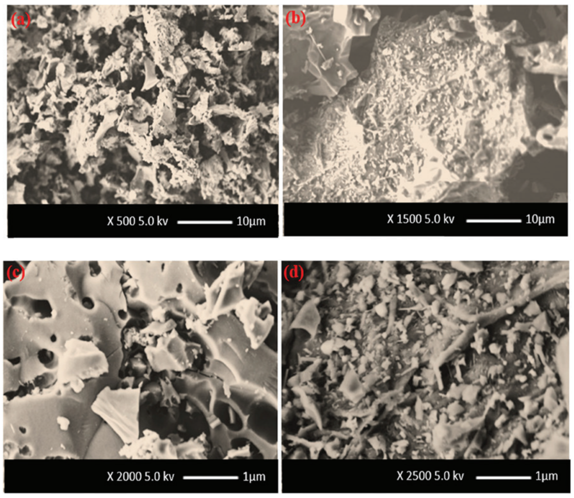

Figure 4. SEM of WNS AND FNWS (Walnut shell)

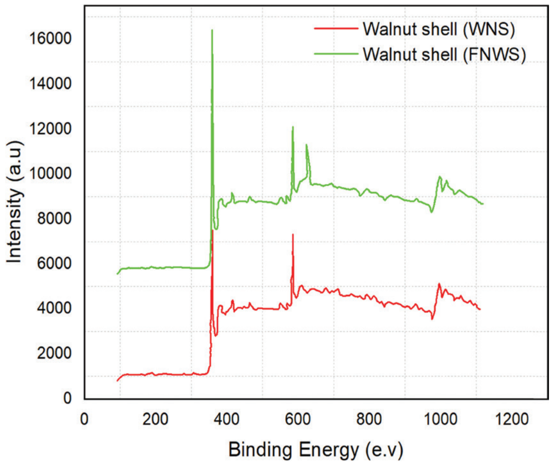

Figure 5. Ferrocene adsorption on walnut shell biochar XPS spectrograph

3.4 XPS SPECTRA

Figure 5 displays the XPS survey scans of WNS and FWNS with and without decreasing graphene oxide. These scans showed the results of the survey. Following adsorption onto WNS and FNWS, rGO (reduced graphene oxide) was also found, as well as notable C (1s), O (1s), and rGO peaks were seen. According to the data, the percentage of C and O on the surface of WSB was 86.2% and 16.4%, respectively. Ferrocene was loaded onto WNS and FNWS as a result of the adsorption of reduced graphene oxide (rGO), and the proportions of C, O, and rGO were found to be 86.9%, 14.5%, and 4.6%, respectively. Therefore, the possible percentage of reduced graphene oxide (rGO) on WNS verifies that WSB is suitable for treating distilled water. The reduced graphene oxide (rGO) adsorption efficiencies of the previously employed biochar, it can be noted that walnut shell biochar (95.6 mg g^{-1}) gave greater rGO (reduced graphene oxide) adsorption.

3.5 TGA ANALYSIS

Figure 6 shows TGA data for 2.5, 5.0, 7.5, and 10 °C/min oxidizing heating rates. There are various phases to weight reduction at these rates. Each TGA curve slope initiates a new thermal event. We see 2.5–7% mass loss at all heating speeds from 29 to 160 °C in the early phase. The highest mass loss in this range is 7% at 5.0°C/min, while the lowest is 2.5% at 2.5°C/min. Moisture and volatile chemicals with poor material bonding cause most loss. The second stage begins at 330°C and lasts till 475°C. At 10°C/min, mass loss is 75-81%; at 5.0 and 7.5°C/min, it's 78-89% and 81-90%, respectively. Maximum heating decrease is 90% at 10 °C/min. This significant loss comes from biochar cellulose and lignin oxidation and devolatilization. Third stage: mass declines slightly after 475 °C, indicating progressive lignin breakdown and a fairly flat TGA curve. Oxidizing biochar may be a solid fuel alternative. While extractives are scarcer, TG curves reveal biochar's primary components, cellulose, hemicellulose, and lignin, breaking down. Cellulose (310-400 °C), hemicellulose (210-325 °C), and lignin break down. Finally, activated pyrolysis zone primary and minor heat processes result from cellulose and hemicellulose breakdown. Final lignin breakdown slows mass loss and creates charcoal residue, especially at 510–800 °C.

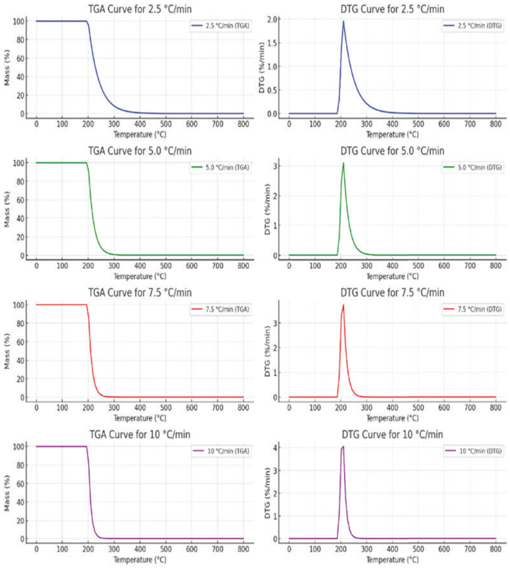

Figure 6. Curves for derivative thermogravimetric analysis (DTG) and thermogravimetric analysis (TGA) for different strains at heating rates of 2.5, 5.0, 7.5, and 10 °C/min

4. THERMAL BEHAVIOR OF BB-PCM ANALYSIS OF MELTING, CONDUCTIVITY, DENSITY, AND DIFFUSIVITY

4.1 ONSET TEMPERATURE AND MELTING TEMPERATURE

Table 2 comprehensively summarizes the experimental thermal characteristics of a composite material of Paraffin Wax, Heated Walnut Shell Powder, and Graphene Nanoparticles. The table explores a range of weight percentages (5%, 10%, 15%, and 20%) and various heat rates (ranging from 2.5°C/min to 10°C/min) in figure 7, shedding light on the material's behavior under diverse conditions. The table offers data on critical parameters, including the onset temperature (T_o), which marks the initiation of the melting process; the melting temperature (T_m), representing complete liquefaction; and the heat of

Table 2. Experimental thermal characteristics of BB-PCM

Heat Rate (°C/min)	**T_o (°C) 5 wt %**	**T_m (°C) 5 wt%**	**T_o (°C) 10 wt %**	**T_m (°C) 10 wt%**	**T_o (°C) 15 wt %**	**T_m (°C) 15 wt%**	**T_o (°C) 20 wt %**	**T_m (°C) 20 wt%**
2.5	59.0	61.3	59.5	62.0	60.0	62.5	60.5	63.0
5.0	59.4	61.7	59.9	62.4	60.4	62.9	60.9	63.5
7.5	59.9	62.4	60.4	63.0	60.9	63.5	61.4	64.0
10	60.3	62.8	60.8	63.4	61.3	63.9	61.8	64.4

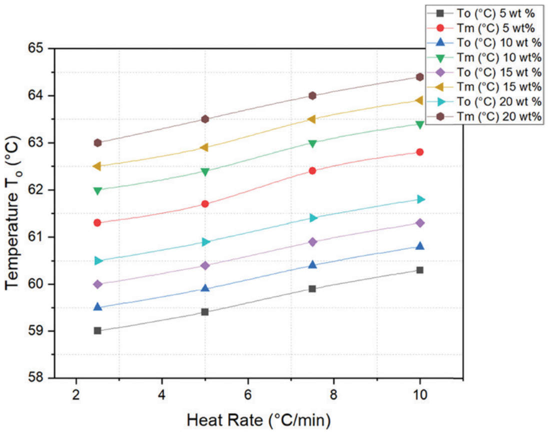

Figure 7. Graph of Onset temperature and melting temperature for BB-PCM at different weight percentages and heat rates

Table 3. (A) Variation of melting enthalpy for BB-PCM

Heat Rate (°C/min)	Melting Enthalpy (J g-1) 5 wt %	Melting Enthalpy (J g-1) 10 wt %	Melting Enthalpy (J g-1) 15 wt %	Melting Enthalpy (J g-1) 20 wt %
2.5	229.8	231.3	232.7	234.3
5.0	232.1	233.6	235.2	235.8
7.5	234.7	236.1	238.7	239.3
10	236.2	238.6	241.2	242.8

Table 3. (B) Thermal Conductivity for BB-PCM

Heat Rate (°C/min)	T_c W/m·K at 5%	T_c W/m·K at 10%	T_c W/m·K at 15%	T_c W/m·K at 20%
2.5	0.44	0.52	0.58	0.63
5.0	0.50	0.60	0.66	0.69
7.5	0.58	0.66	0.74	0.77
10	0.68	0.76	0.83	0.84

Table 3. (C) Density of for BB-PCM

Heat Rate (°C/min)	Density(g/cm³) at 5%	Density(g/cm³) at 10%	Density(g/cm³) at 15%	Density (g/cm³) at 20%
2.5	0.85	0.84	0.87	0.91
5.0	0.87	0.86	0.89	0.93
7.5	0.88	0.89	0.91	0.95
10	0.91	0.91	0.93	0.96

Table 3: (D) Thermal Diffusivity BB-PCM

Heat Rate (°C/min)	Thermal Diffusivity (mm²/s) at 5%	Thermal Diffusivity (mm²/s) at 10%	Thermal Diffusivity (mm²/s) at 15%	Thermal Diffusivity (mm²/s) at 20%
2.5	0.22	0.26	0.28	0.31
5.0	0.25	0.29	0.31	0.34
7.5	0.28	0.32	0.34	0.37
10	0.31	0.35	0.37	0.41

fusion (ΔHm), indicating the energy required to melt one gram of the material. Heat rate impacts fusion heat but not start or melting temperatures. The heat of fusion is more affected by paraffin wax composite weight percentage than onset and melting. Graphene Nanoparticles with Heated Walnut Shell Powder paraffin wax melts hotter than pure paraffin. Nucleating Walnut Shell Powder with Graphene Nanoparticles strengthens solid crystal formation. Nucleating agents diminish crystallization energy barriers, raising onset and melting temperatures. Due to its higher heat of fusion, melting paraffin wax composite requires more energy than pure paraffin. BB-PCM's thermal characteristics enable thermal storage, phase change material thermal management, and self-healing material development.

4.2 MELTING ENTHALPY

Table 3 (a) presents a detailed comparison of the melting enthalpy (in J g^{-1}) for three different composite materials, namely BB-PCM (Paraffin Wax with Heated Walnut Shell Powder and Graphene Nanoparticles). The data varies across weight percentages (5% to 20%) and different heat rates (2.5°C/min to 10°C/min). With composite material weight %, all heating speeds increase melting enthalpy. Composite phase transition heat absorption and melting enthalpy increase with powder and nanoparticle concentrations. Walnut shell powder and graphene nanoparticle nucleation raise composite melting temperatures with weight %. Nucleating agents increase melting temperatures and crystallization. Powder and graphene nanoparticle melting enthalpy increases with weight % because they have higher thermal conductivity than paraffin wax. Composites absorb more heat before phase transition with improved thermal conductivity. Depending on weight %, heat rate, powders, and nanoparticles, this composites' melting enthalpy and temperature can store and manage heat. Figure 8(a) shows these composites' melting enthalpy with varying heat rates and weight percentages.

4.3 THERMAL CONDUCTIVITY

Table 3 (b) provides a comprehensive comparison of the thermal conductivity (measured in W/m·K) for three different BB-PCM (Phase Change Materials) compositions, each containing Paraffin Wax combined with various additives, including Heated Walnut Powder and Graphene Nanoparticles. The data is presented across different heat rates (ranging from 2.5°C/min to 10°C/min) and varying weight percentages (5%, 10%, 15%, and 20%). Thermal conductivity increases with weight percentage in BB-PCM composition. Higher concentrations of additives like walnut powder and graphene nanoparticles improve the composite's heat conductivity. For each composition, thermal conductivity improves with heat rate, showing that a faster heating process improves heat conductivity. The choice of additives significantly affects the thermal conductivity of composite materials. Figure 8 (b) shows the thermal conductivity of BB-PCM compositions at different heat rates to supplement the table. These results help explain how these composites can be customized for heat conduction and management applications.

4.4 DENSITY

Table 3 (c) provides a detailed comparison of the experimental densities (measured in g/cm³) for three different BB-PCM (Phase Change Materials) compositions, each consisting of Paraffin Wax blended with different additives, including Heated Walnut Powder and Graphene Nanoparticles. The data is presented for various heat rates (ranging from 2.5°C/min to 10°C/min) and different weight percentages (5%, 10%, 15%, and 20%). Density tends to increase with higher weight percentages for all three BB-PCM compositions. This indicates that a greater concentration of additives, walnut powder, and graphene nanoparticles leads to higher composite densities. As the heat rate increases, there is an overall increase in density for each composition, suggesting that a faster heating process tends to result in higher material densities. This illustrates that the choice of additives significantly influences the density of the composite materials. Figure 8 (c) visually represents the comparison of densities for these BB-PCM compositions at different heat rates.

4.5 THERMAL DIFFUSIVITY

Table 3 (d) compares thermal diffusivity (mm²/s) for three BB-PCM compositions, each made of Paraffin Wax and various additives. Heat rates (2.5°C/min to 10°C/min) and weight percentages (5%, 10%, 15%, and 20%) are shown. Weight % enhances thermal diffusivity in BB-PCM pairings. Higher quantities of graphene nanoparticles and additions like powdered walnut increase thermal diffusivity, speeding heat propagation. Heat rate increases thermal diffusivity in each composition. Faster heating enhances material heat transfer. The graphene nanoparticle-heated walnut shell powder composite has the highest thermal diffusivity of the three BB-PCM compositions. This implies that additive selection greatly impacts composite thermal diffusivity. Thermal diffusivity for various BB-PCM compositions at varied weight percentages and heat rates is shown in Figure 8 (d).

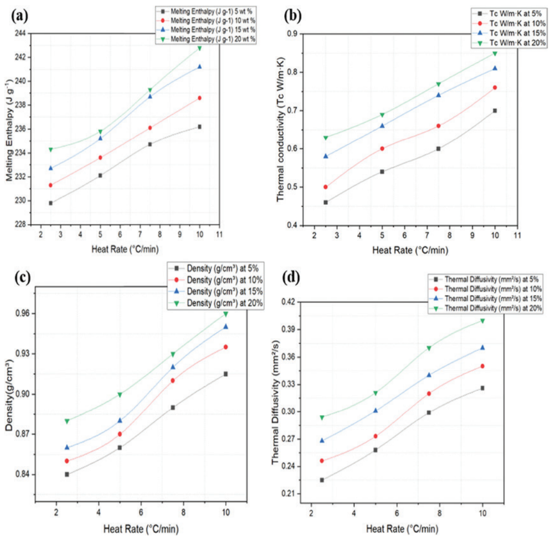

Figure 8. (a) Variation of melting enthalpy, (b) thermal conductivity, (c) density, and (d) thermal diffusivity of different Bio-Based Phase Change Materials (BB-PCM) at various heat rates and weight percentages

5. CONCLUSION

In conclusion, paraffin wax composites enriched with heated walnut shell powder and graphene nanoparticles were prepared and measured for thermal conductivity, melting temperature, and enthalpy at different heating rates and weight percentages to reveal composite materials' thermal properties. A thorough approach comprising exact weighing, blending, and characterisation revealed how additives affect composite thermal performance. Heated walnut shell powder, a renewable and biodegradable material, and graphene nanoparticles improve paraffin wax composites' thermal conductivity and heat capacity. The weight proportion of additions preserves crystallinity, as shown by X-ray diffraction examination of crystalline formations with different compositions.

Walnut shell functional groups and acid treatment affected surface characteristics in FTIR survey. scanning electron micrographs indicated heat transfer and pollutant absorption from the composites' porous structure. XPS demonstrated graphene nanoparticles on composite surfaces enhancing adsorption and thermal conductivity. A thermogravimetric investigation indicated discrete deterioration stages in the composites, indicating thermal stability and solid fuel alternatives.

Thermal conductivity, density, melting enthalpy, and thermal diffusivity investigations at different weight percentages and heating speeds showed additive effects. Additives increased density, melting enthalpy, and thermal conductivity. Our investigation of paraffin wax composites with heated walnut shell powder and graphene nanoparticles shows how it can store thermal energy, manage temperature, and absorb pollutants. Processing and elemental studies may improve industrial and environmental thermal properties. Naval engineering is changing using bio-based nano-phase transition materials. Eco-friendly materials store and control thermal energy in many heating and cooling systems, waste heat recovery, and engine cooling. Key components can survive longer with biocompatible corrosion-resistant coatings. Desalination, abundance control, and underwater acoustics. Research predicts these environmentally friendly PCMs will increase maritime engineering efficiency and sustainability, despite their cost, durability, and uniformity.

6. REFERENCES

1. ALKHAZALEH, A.H., 2020. Preparation and characterization of isopropyl palmitate/expanded perlite and isopropyl palmitate/nanoclay composites as form-stable thermal energy storage materials for buildings. J Energy Storage 32. https://doi.org/10.1016/j.est.2020.101679
2. ASLFATTAHI, N., SAIDUR, R., ARIFUTZZAMAN, A., SADRI, R., BIMBO, N., SABRI, M.F.M., MAUGHAN, P.A.,

BOUSCARRAT, L., DAWSON, R.J., SAID, S.M., GOH, B.T., SIDIK, N.A.C., 2020. Experimental investigation of energy storage properties and thermal conductivity of a novel organic phase change material/MXene as A new class of nanocomposites. J Energy Storage 27. https://doi.org/10.1016/j.est.2019.101115

3. ATINAFU, D.G., CHANG, S.J., KIM, S., 2020a. Infiltration properties of n-alkanes in mesoporous biochar: The capacity of smokeless support for stability and energy storage. J Hazard Mater 399. https://doi.org/10.1016/j.jhazmat.2020.123041
4. ATINAFU, D.G., JIN CHANG, S., KIM, K.H., KIM, S., 2020B. Tuning surface functionality of standard biochars and the resulting uplift capacity of loading/energy storage for organic phase change materials. Chemical Engineering Journal 394. https://doi.org/10.1016/j.cej.2020.125049
5. BAYLIS, C., CRUICKSHANK, C.A., 2023. Review of bio-based phase change materials as passive thermal storage in buildings. Renewable and Sustainable Energy Reviews. https://doi.org/10.1016/j.rser.2023.113690
6. CÁRDENAS-RAMÍREZ, C., JARAMILLO, F., GÓMEZ, M., 2020. Systematic review of encapsulation and shape-stabilization of phase change materials. J Energy Storage. https://doi.org/10.1016/j.est.2020.101495
7. CHEN, K., YU, X., TIAN, C., WANG, J., 2014. Preparation and characterization of form-stable paraffin/polyurethane composites as phase change materials for thermal energy storage. Energy Convers Manag 77. https://doi.org/10.1016/j.enconman.2013.09.015
8. DA CUNHA, S.R.L., DE AGUIAR, J.L.B., 2020. Phase change materials and energy efficiency of buildings: A review of knowledge. J Energy Storage. https://doi.org/10.1016/j.est.2019.101083
9. DENG, J.J., SONG, L.Y., XU, J., LIU, B., LU, J.S., ZHANG, J.W., 2020. Characteristics of Heat Transfer During Cooling Down Process in a Single Cargo Tank of LNG Carrier. International Journal of Maritime Engineering 162. https://doi.org/10.3940/rina.ijme.2020.a3.588
10. DERE, C., DENIZ, C., 2019. Energy efficiency based operation of compressed air system on ships to reduce fuel consumption and CO2 emission. Transactions of the Royal Institution of Naval Architects Part A: International Journal of Maritime Engineering 161. https://doi.org/10.3940/rina.ijme.2019.a2.532
11. FENG, L., ZHENG, J., YANG, H., GUO, Y., LI, W., LI, X., 2011. Preparation and characterization of polyethylene glycol/active carbon composites as shape-stabilized phase change materials. Solar Energy Materials and Solar Cells 95. https://doi.org/10.1016/j.solmat.2010.09.033
12. HOCK, P.E., ZAINI, M.A.A., 2018. Activated carbons by zinc chloride activation for dye removal – a commentary. Acta Chimica Slovaca 11. https://doi.org/10.2478/acs-2018-0015
13. HUANG, X., ALVA, G., LIU, L., FANG, G., 2017. Preparation, characterization and thermal properties of fatty acid eutectics/bentonite/expanded graphite composites as novel form–stable thermal energy storage materials. Solar Energy Materials and Solar Cells 166. https://doi.org/10.1016/j.solmat.2017.03.026
14. JEON, J., PARK, J.H., WI, S., YANG, S., OK, Y.S., KIM, S., 2019. Characterization of biocomposite using coconut oil impregnated biochar as latent heat storage insulation. Chemosphere 236. https://doi.org/10.1016/j.chemosphere.2019.06.239
15. JEONG, S.G., CHUNG, O., YU, S., KIM, SUGHWAN, KIM, SUMIN, 2013. Improvement of the thermal properties of Bio-based PCM using exfoliated graphite nanoplatelets. Solar Energy Materials and Solar Cells 117. https://doi.org/10.1016/j.solmat.2013.05.038
16. LEE, H.W., LEE, H., KIM, Y.M., PARK, R. SU, PARK, Y.K., 2019. Recent application of biochar on the catalytic biorefinery and environmental processes. Chinese Chemical Letters 30. https://doi.org/10.1016/j.cclet.2019.05.002
17. LI, D., ZHUANG, B., CHEN, Y., LI, B., LANDRY, V., KABOORANI, A., WU, Z., WANG, X.A., 2022. Incorporation technology of bio-based phase change materials for building envelope: A review. Energy Build. https://doi.org/10.1016/j.enbuild.2022.111920
18. LIU, L., FAN, X., ZHANG, Y., ZHANG, S., WANG, W., JIN, X., TANG, B., 2020. Novel bio-based phase change materials with high enthalpy for thermal energy storage. Appl Energy 268. https://doi.org/10.1016/j.apenergy.2020.114979
19. LIU, L., PENG, B., YUE, C., GUO, M., ZHANG, M., 2019. Low-cost, shape-stabilized fly ash composite phase change material synthesized by using a facile process for building energy efficiency. Mater Chem Phys 222. https://doi.org/10.1016/j.matchemphys.2018.09.072
20. LU, X., HUANG, J., WONG, W.Y., QU, J. PING, 2019. A novel bio-based polyurethane/wood powder composite as shape-stable phase change material with high relative enthalpy efficiency for solar thermal energy storage. Solar Energy Materials and Solar Cells 200. https://doi.org/10.1016/j.solmat.2019.109987
21. NAVARRO, L., BARRENECHE, C., CASTELL, A., REDPATH, D.A.G., GRIFFITHS, P.W., CABEZA, L.F., 2017. High density polyethylene spheres with PCM for domestic hot water applications: Water tank and laboratory scale study. J Energy Storage 13. https://doi.org/10.1016/j.est.2017.07.025

22. NICHOLAS, A.F., HUSSEIN, M.Z., ZAINAL, Z., KHADIRAN, T., 2018. Palm kernel shell-activated carbon as an inorganic framework for shape-stabilized phase change material. Nanomaterials 8. https://doi.org/10.3390/nano8090689
23. RANJBAR, S.G., ROUDINI, G., BARAHUIE, F., 2020. Fabrication and characterization of phase change material-SiO2 nanocomposite for thermal energy storage in buildings. J Energy Storage 27. https://doi.org/10.1016/j.est.2019.101168
24. ROSSI, J.E., SCHAUERMAN, C.M., LAWLOR, C.C., CRESS, C.D., GANTER, M.J., BUCOSSI, A.R., LANDI, B.J., 2022. Carbon nanotube survivability in marine environments and method for biofouling removal. Biofouling 38. https://doi.org/10.1080/08927014.2022.2102904
25. SHAN, R., HAN, J., GU, J., YUAN, H., LUO, B., CHEN, Y., 2020. A review of recent developments in catalytic applications of biochar-based materials. Resour Conserv Recycl. https://doi.org/10.1016/j.resconrec.2020.105036
26. TANG, Y., JIA, Y., ALVA, G., HUANG, X., FANG, G., 2016. Synthesis, characterization and properties of palmitic acid/high density polyethylene/graphene nanoplatelets composites as form-stable phase change materials. Solar Energy Materials and Solar Cells 155. https://doi.org/10.1016/j.solmat.2016.06.049
27. WANG, C., LIANG, W., YANG, Y., LIU, F., SUN, H., ZHU, Z., LI, A., 2020. Biomass carbon aerogels based shape-stable phase change composites with high light-to-thermal efficiency for energy storage. Renew Energy 153. https://doi.org/10.1016/j.renene.2020.02.008
28. WU, X., LV, Y., 2022. Study on the Corrosion Resistance of Laser Clad Al0.7FeCoCrNiCux High-Entropy Alloy Coating in Marine Environment. Coatings 12. https://doi.org/10.3390/coatings12121855
29. YADAV, V., SINGH, S., CHAUDHARY, N., GARG, M.P., SHARMA, S., KUMAR, A. AND LI, C., 2023. Dry sliding wear characteristics of natural fibre reinforced poly-lactic acid composites for engineering applications: Fabrication, properties and characterizations. *Journal of Materials Research and Technology*, *23*, pp.1189-1203.
30. YANG, H., WANG, Y., YU, Q., CAO, G., SUN, X., YANG, R., ZHANG, Q., LIU, F., DI, X., LI, J., WANG, C., LI, G., 2018. Low-cost, three-dimension, high thermal conductivity, carbonized wood-based composite phase change materials for thermal energy storage. Energy 159. https://doi.org/10.1016/j.energy.2018.06.207
31. ZHANG, N., ZHAO, Z., 2020. Research and analysis on the improvement of the salt corrosion resistance of concrete by a kind of micro and nano composite coating material with double rough structure. Academic Journal of Manufacturing Engineering 18.
32. ZHANG, X., HUANG, Z., YIN, Z., ZHANG, W., HUANG, Y., LIU, Y., FANG, M., WU, X., MIN, X., 2017. Form stable composite phase change materials from palmitic-lauric acid eutectic mixture and carbonized abandoned rice: Preparation, characterization, and thermal conductivity enhancement. Energy Build 154. https://doi.org/10.1016/j.enbuild.2017.08.057
33. ZHONG, W., ZHANG, D., WANG, Y., ZHAO, Y., LIU, J., 2022. Analysis of engineering application requirements of nano-coating materials, in Journal of Physics: Conference Series. https://doi.org/10.1088/1742-6596/2194/1/012012